



Crustal flow pattern beneath the Tibetan Plateau constrained by regional Lg-wave Q tomography



Lian-Feng Zhao^{a,*}, Xiao-Bi Xie^b, Jian-Kun He^c, Xiaobo Tian^a, Zhen-Xing Yao^a

^a Key Laboratory of the Earth's Deep Interior, Institute of Geology and Geophysics, Chinese Academy of Sciences, Beijing, China

^b Institute of Geophysics and Planetary Physics, University of California at Santa Cruz, CA, USA

^c Key Laboratory of Continental Collision and Plateau Uplift, Institute of Tibetan Plateau Research, Chinese Academy of Sciences, Beijing, China

ARTICLE INFO

Article history:

Received 3 May 2013

Received in revised form 19 September 2013

Accepted 19 September 2013

Available online xxx

Editor: P. Shearer

Keywords:

Lg attenuation

Q tomography

lower-crustal flow

Tibetan Plateau

crustal deformation

ABSTRACT

As a prominent geophysical anomaly, unusually high seismic wave attenuation is observed in the crust and upper mantle of the Tibetan Plateau, particularly along its northern area. Theoretical and laboratory investigations show that the strong seismic attenuation can indicate high temperatures and partial melting, which may decrease the viscosity of the material and cause it to flow. Thus, seismic attenuation distribution may provide useful constraints to the crust flows if they exist. Using Lg-wave Q tomography, we construct a 0.05–10.0 Hz broadband high-resolution crust attenuation model for the Tibetan Plateau and its surrounding regions. The maximum spatial resolution is approximately $1.0^\circ \times 1.0^\circ$ in well-covered areas and for frequencies between 0.05 and 1.5 Hz. This attenuation model reveals an apparent low- Q_{Lg} belt stretching along the northern and eastern Tibetan plateau. Combining the Lg-wave Q model with other geophysical data, two possible crust flow channels are found in the Tibetan Plateau. The main flow channel is from north to east and then turns to southeastern Tibet along the western edge of the rigid Sichuan basin, while a second channel starts from southern Tibet and crosses the Eastern Himalayan syntaxis.

© 2013 Published by Elsevier B.V.

1. Introduction

A lower-crust flow model can explain many geological and geophysical observations in the Tibetan Plateau. Moreover, these observations provide important constraints to the dynamic processes in this region (Klemperer, 2006; Royden et al., 2008; Searle et al., 2011). Typically, the surface strain rates from the Global Positioning System (GPS) and earthquake data are consistent with a gravitationally driven flow model of a viscous lithosphere bounded by strong converging blocks in northern and southern Tibet (e.g., Clark and Royden, 2000; Flesch et al., 2001; Heidbach et al., 2010; Zhang et al., 2004). The low Pn velocities, inefficient Sn propagation, high Poisson's ratios of approximately 0.35, and high seismic Lg-wave attenuation are observed in northern Tibet, suggesting that partial melting is existed within the crust of this region (Fan and Lay, 2003b; Nelson et al., 1996; Owens and Zandt, 1997; Rodgers and Schwartz, 1998). The seismic and magnetotelluric observations revealed that, in eastern and southeastern Tibetan plateau, there are low-velocity and high-conductivity layers in the middle- and lower-crusts, which support a lower-crust flow model (e.g., Bai et al., 2010; Liu et al., 2006; Unsworth et al., 2005;

Xu et al., 2007; Yao et al., 2008). However, whether the crust flow is widely spread throughout the entire Tibetan Plateau or is limited to certain narrow geological channels is still under debate. To explore the lower-crust flow pattern throughout the Tibetan Plateau, high-resolution regional measurements of the crust physical properties, such as the velocity, attenuation, anisotropy and electrical structures, are required (e.g., Fan and Lay, 2002; Li et al., 2008; Shapiro et al., 2004; Wang et al., 2013).

Seismic attenuation is usually an indicator of high temperatures and partial melts. An unusually high attenuation in both the crust and upper mantle is one of the first geophysical anomalies discovered in Tibet, particularly in its northern region. The strong Pnl- and Lg-wave attenuations are consistent with the strong Sn-wave attenuation in this region (Fan and Lay, 2003b; Ni and Barazangi, 1983; Rodgers and Schwartz, 1998). Both Rodgers and Schwartz (1998) and Fan and Lay (2003b) suggested that the strong attenuation results from widespread partial melting in the northern Tibetan crust. Xie et al. (2004) found strong crustal Lg-wave attenuation in the Yangbajing graben in southern Tibet and attributed the attenuation to hydrothermal and magmatic fluid activities in the upper-crust. Based on deep seismic sounding data from eastern Tibet, Wang et al. (2007) compared the amplitude difference of seismic PmP waveforms between the observed and synthetic data. They suggested that the weak PmP amplitudes were resulted from a high attenuation in the lower crust and hence suggested

* Corresponding author. Tel.: +86 10 82998658; fax: +86 10 62010846.

E-mail addresses: zhaolf@mail.iggcas.ac.cn (L.-F. Zhao), xxie@ucsc.edu (X.-B. Xie), jkhe@itpcas.ac.cn (J.-K. He).

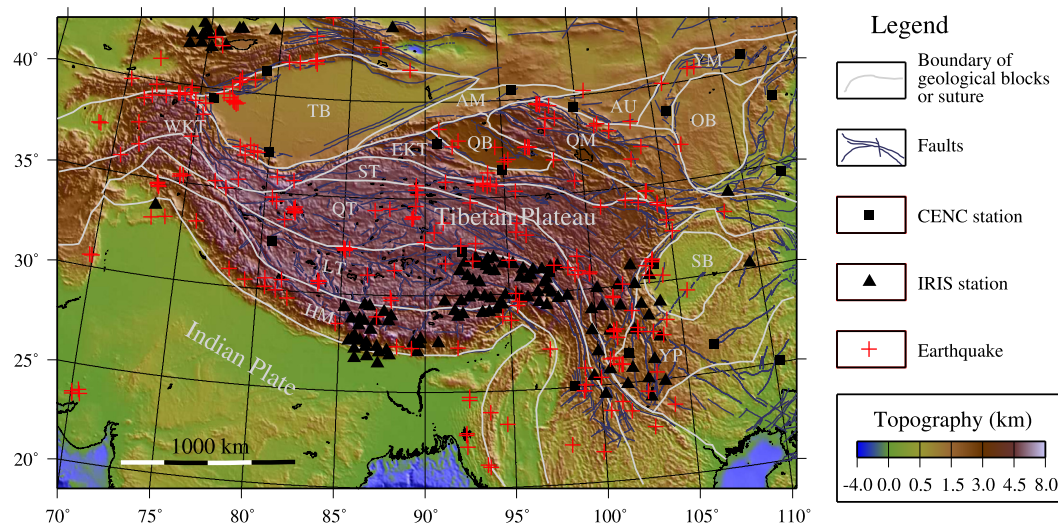


Fig. 1. A topographic map superimposed with main fault systems (light-blue lines), regional tectonics in the Tibetan plateau and its surrounding regions, the locations of the CENC (solid squares) and IRIS (triangles) stations, and the epicenters of selected earthquakes (crosses) used in this study. The information about the major geo-blocks is also listed in Table 1.

that a lower-crust flow was likely existed in this region. In the Tibetan Plateau, previous attenuation studies were mostly limited within local regions or to very low resolutions because of limited data (Bao et al., 2011; Fan and Lay, 2002, 2003a, 2003b; McNamara et al., 1994; Rodgers and Schwartz, 1998; Xie, 2002; Xie et al., 2004; Zhou et al., 2011). Until recently, due to the lack of a high-resolution attenuation model for the Tibetan Plateau, it has been difficult to link the attenuation information with the regional tectonics.

In this study, we develop a high-resolution Lg-wave attenuation model in the Tibetan Plateau and its adjacent regions and investigate its connections to the thermal activities and possible material movement in the lower crust and upper mantle.

2. Data and methods

We collected 7545 broadband vertical-component digital seismograms recorded at 146 stations from 232 regional earthquakes between January 2001 and June 2008 with their ray paths penetrating the plateau. The waveforms were obtained from the China Earthquake Networks Center (CENC) and the Incorporated Research Institutions for Seismology (IRIS) consortium. The station parameters, including code, location, data resource, and affiliation, are listed in Tables S1 and S2 in the supplementary document. Both the CENC and the IRIS stations are equipped with broadband instruments having nearly flat velocity responses from 0.03 Hz to 8.0 Hz and one of the three sampling rates: 20, 40 and 50 points per second. The earthquake parameters are listed in Table S3 in the supplementary document. Shown in Fig. 1 is a topographic map overlapped with the main fault systems (light-blue lines), geotectonics (white lines), locations of the CENC (solid squares) and IRIS (triangles) stations, and epicenters of the earthquakes (crosses) used in this study. The waveforms were selected based on the criteria that these earthquakes were located in the crust, with their magnitudes ranged between $m_b = 3.5$ and 6.0, and the epicenter distances were between 200 and 3000 km. Shown in Figs. S1 and S2 are sample records from an earthquake occurred on June 29, 2002, with S1 filtered between 0.2–2.0 Hz and S2 filtered between 1.0–10.0 Hz. At lower frequencies, the scattering generated P-coda waves are much weaker than at high frequencies.

The data pre-processing was conducted following Zhao et al. (2010, 2013). We extracted the Lg-waveforms using a group-velocity window of 3.6–3.0 km/s and collected the noise time

series in an equal-length window as the Lg phase before the first-arriving P wave. Then, we calculated Fourier spectra for both the Lg-wave and the noise, sampled the spectral amplitudes, and corrected for the noise effects. As an example, Fig. 2 illustrates this process for event 2004/08/26 at station MC10. In Fig. 2a, the solid and dashed lines denote the amplitude spectra of Lg and pre-P noise, where the circles and triangles denote the samples at 58 frequencies distributed log evenly between 0.05 and 10.0 Hz. From the signal and noise spectral amplitudes, we calculated the signal-to-noise ratios at individual frequencies (shown in Fig. 2b as solid circles). A threshold of 2.0 is shown as a dashed line and was used for rejecting the low quality data. The noise-corrected Lg-wave spectrum is illustrated in Fig. 2c, where points below the threshold are dropped. After batch processing all regional waveforms, we obtained the source-station amplitudes at individual frequencies between 0.05 and 10.0 Hz. Following Xie et al. (2004) and Zhao et al. (2013), we extracted the interstation (dual-station) data for individual frequencies from the source-station (single-station) data. Both dual- and single-station data were used in the joint inversion for the Lg Q distribution and Lg-wave source functions (for details see Zhao et al., 2013). Using a checkerboard method (e.g., Zhao et al., 2013) with variable grid sizes from $0.8^\circ \times 0.8^\circ$ to $2^\circ \times 2^\circ$, we conducted resolution analyses independently for individual frequencies. At each frequency, we combined $\pm 7\%$ checkerboard shaped perturbations to a constant background Q model, and used it to generate a spectra data set. To simulate the noise in real data, a 5% root mean square random noise was added to the spectra data. We then used this synthetic data set as the input of the inversion system and the inverted result was compared to the checkerboard model to estimate the resolution. Fig. 2d summarizes the number of available rays (for dual-station, single-station, and combined data sets) versus frequency, where the shaded areas illustrate the estimated resolutions for particular frequencies.

3. Tomographic model of Lg attenuation

Based on the above mentioned Lg dataset, we obtained a broadband attenuation model for the Tibetan Plateau and its surrounding regions, where Q_{Lg} is distributed geographically as well as at 58 discrete frequencies between 0.05 and 10.0 Hz.

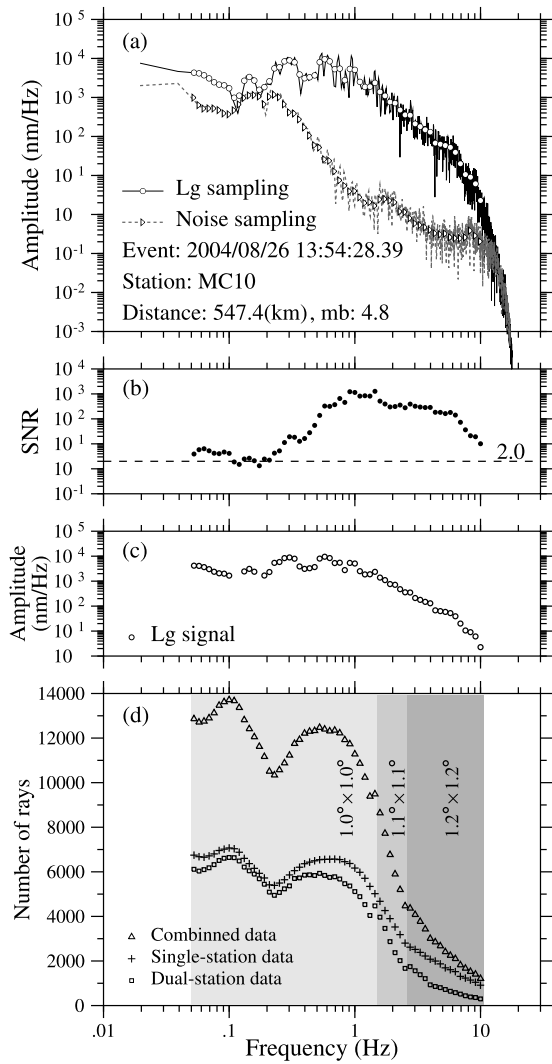


Fig. 2. Summary on Lg-wave data processing. As an example, shown here are (a) raw Lg-wave spectra (circles) and noise spectra (triangles) recorded at station MC10 from earthquake 2004/08/26, (b) signal-to-noise ratios (SNR), (c) noise-corrected Lg-wave spectra, and (d) the numbers of available rays at individual frequencies along with the estimated resolutions marked by shaded areas. The dashed line in (b) is the threshold used to eliminate the data with SNR below 2.0.

3.1. Q_{Lg} maps at individual frequencies

Figs. 3a–3c illustrate the Q_{Lg} distributions at 0.5, 1.0, and 2.0 Hz, respectively, along with the major geological sutures (white lines) and active fault systems (thin black lines). Note that different color scales are used for these Q_{Lg} images. The most prominent feature in these maps is that the high-frequency Q_{Lg} is generally higher than the lower-frequency values. The lateral Q_{Lg} variations are consistent with regional tectonics. Compared to its surrounding areas, the Tibetan Plateau is characterized by strong Lg-wave attenuations, with low- Q_{Lg} zones seen in the Songpan–Ganzi–Hoh xil (ST), Qiangtang (QT), and Lhasa Terrane (LT) regions, forming a belt first from west to east then turn to south. Shown in Fig. 3d are some 1 Hz Q_{Lg} measurements from previous investigators (Fan and Lay, 2002, 2003a, 2003b; Rai et al., 2009; Xie, 2002; Xie et al., 2004; Zhao et al., 2013). Comparison between Figs. 3b and 3d demonstrates that our result is consistent with the previous measurements but with higher resolution and better coverage. Shown in Figs. 3e and 3f are the ray-path coverage and the checkerboard resolution analyses at 1 Hz. In well-covered areas, the spatial resolution can reach to $1^\circ \times 1^\circ$ or higher.

There are strong Q_{Lg} variations between different geology formations as well as within each unit. We investigated the Lg attenuation in different geological formations by calculating their average values (Zhao et al., 2010, 2013). The geographically averaged Q_{Lg} values versus frequency in selected tectonic regions are shown in Fig. 4. As an example, the light gray crosses in Fig. 4a are the inverted Q_{Lg} values within the Songpan–Ganzi–Hoh xil terrane (ST). The result reveals the Q_{Lg} –frequency relationship but with large scatters. We calculated the mean Q_{Lg} values within narrow frequency bands, and the results are shown as squares with error bars. These statistical results are more robust in characterizing the regional variations and frequency dependence of Q_{Lg} . Also labeled in Fig. 4a are the average Q_0 and its standard deviations. Fig. 4b summarizes the average Q_{Lg} versus frequency relations for selected geological blocks, and these results are also listed in Table 1. The average Q_{Lg} values between 0.2 and 2.0 Hz (shaded area in Fig. 4b) show larger regional variations, thus suitable for characterizing the regional attenuation variations. The part of Tibetan Plateau with elevations above 4000 m have an average Q_0 of 280 (194–406), much lower than the values of 374 (273–512) and 414 (232–739) from North China Craton (NCC) and North-east China (NEC) (Zhao et al., 2010, 2013). The regions surrounding the Tibetan plateau are mostly characterized by high Q_0 values (Tarim basin: 433, Altyn Tagh mountain: 517, Qaidam basin: 385, Alashan uplift: 452, Yinshan mountains: 444, Ordos: 395, and Sichuan basins: 456) except for Yungui Plateau, which has a relatively low Q_0 of 247.

3.2. Broadband Q_{Lg} images

To explore the relationship between the broadband Q_{Lg} and the regional geology, we use cross-sections to show the frequency dependence of the attenuation. Shown in Fig. 5 are six east–west cross-sections located at selected latitudes from north to south. In each panel, the upper part compares the Q_{Lg} (0.2–2.0 Hz) (average Q_{Lg} between 0.2 and 2.0 Hz), surface topography, and Moho depths from CRUST2.0 (Bassin et al., 2000), and the lower part shows Q_{Lg} versus frequency along the section. For these cross sections, their latitudes are labeled in the panel, and the longitudes are indicated along the top and bottom. Also labeled in these sections are names of major geology blocks and the locations where minimum Q_{Lg} appears (with arrows). Located in the northernmost portion of the Tibetan Plateau, the section along the 37.5° N latitude passes sequentially through the Tarim basin (TB), Eastern Kunlunshan terrane (EKT), Qaidam basin (QB), Qilian-shan mountains (QM), and Ordos basin (OB). As shown in Fig. 5a, there are two apparent low- Q regions, EKT and QM, corresponding to mountain areas, while the three stable basins have relatively higher Q_{Lg} values (as can be seen from Fig. 3). The 35° N latitude section crosses the Qiangtang (QT), Songpan–Ganzi–Hoh xil (ST), and Eastern Kunlunshan Terranes (EKT). Located in the North Tibetan Plateau, the crust in this region was suggested by Owens and Zandt (1997) to be partially melted due to high temperatures, thus having relatively low Q_{Lg} . In Fig. 5b, low- Q_{Lg} anomalies occur near 89° E and 95° E, which agrees with the findings by Fan and Lay (2002, 2003a, 2003b). The 32.5° N latitude section traverses the Qiangtang (QT) and Songpan–Ganzi–Hoh xil terranes (ST) and enters into the Sichuan basins (SB). Relatively low- Q_{Lg} values are observed in eastern Tibet as shown by arrows in Fig. 5c. Located in the south Tibetan Plateau, section along the 30° N latitude sequentially passes through the Himalaya (HM), Lhasa (LT), Qiangtang (QT), and Songpan–Ganzi–Hoh xil terranes (ST) and the Sichuan basins (SB). In Fig. 5d, sections along 30° N latitude show

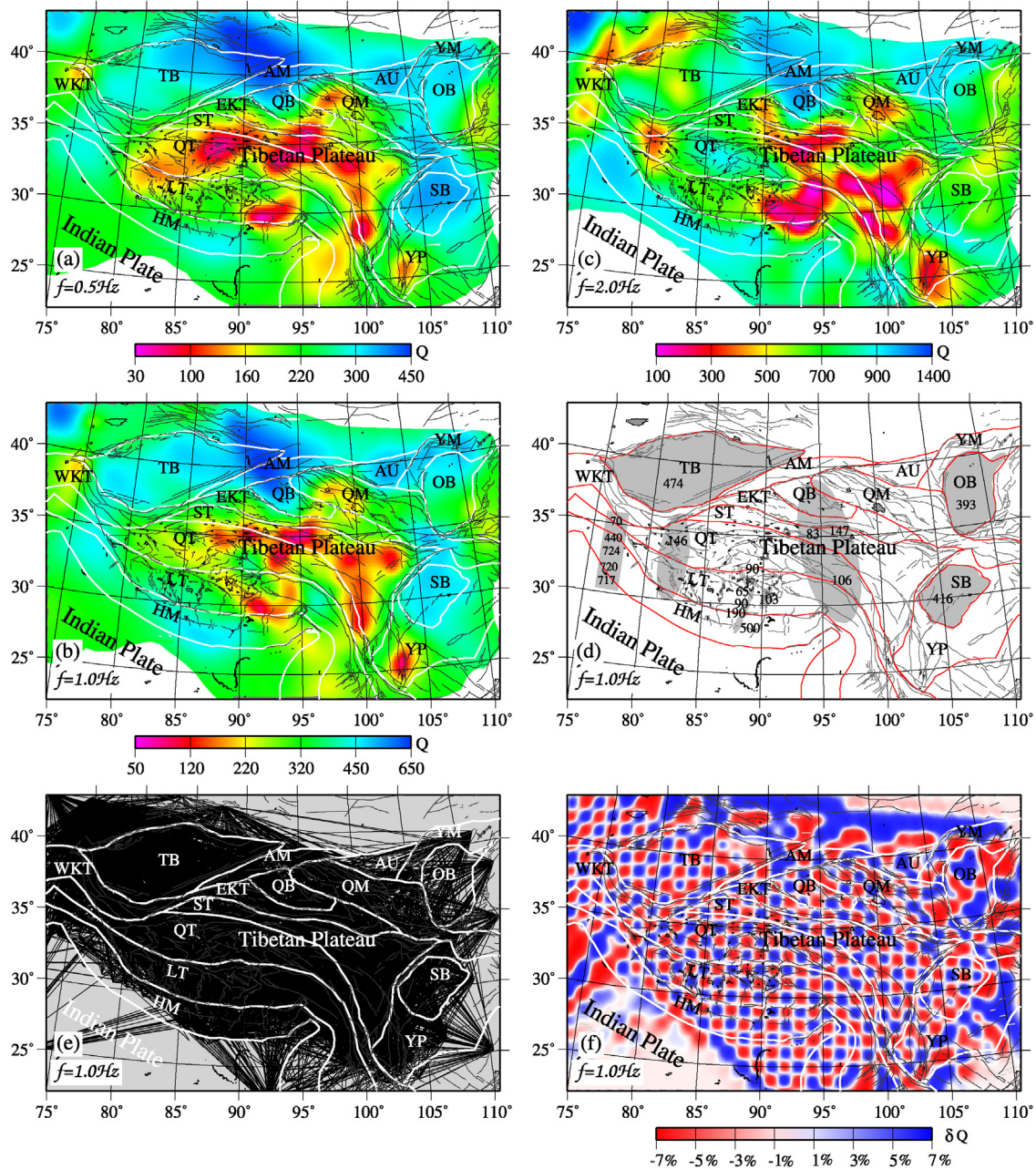


Fig. 3. Selected Q_{Lg} maps compared with previous investigations. (a)–(c) Q_{Lg} maps at 0.5 Hz, 1.0 Hz and 2.0 Hz, (d) a schematic map showing Lg Q measurements from previous investigations, (e) 1 Hz ray coverage, and (f) checkerboard resolution analyses. Also illustrated in the figures are geological boundaries (white or red lines) and the fault systems (thin black lines).

apparently strong attenuation regions between 90° and 95° E in southern Tibet and near 100° E in southeast Tibet. Geophysical anomalies such as middle-crustal low-velocity, low- Q_{Lg} , high-heat flows and crustal electrical conductivities have been observed in southern Tibet (e.g., Langille et al., 2010; Wei et al., 2001; Xie et al., 2004; Zhang et al., 2011). The partial melting, resulting from collisional crustal thickening, is thought to be responsible for these geological anomalies (e.g., Beaumont et al., 2004; Nelson et al., 1996). The southeastern Tibet, the Burma arc, and Yungui plateau (YP) are also characterized by strong attenuation in the crust, as shown in Figs. 5e and 5f. It is commonly accepted that this region is an exit of the lower crust channel flow in eastern Tibet (e.g., Clark and Royden, 2000; Royden et al., 2008; Wang et al., 2013; Zhang et al., 2010).

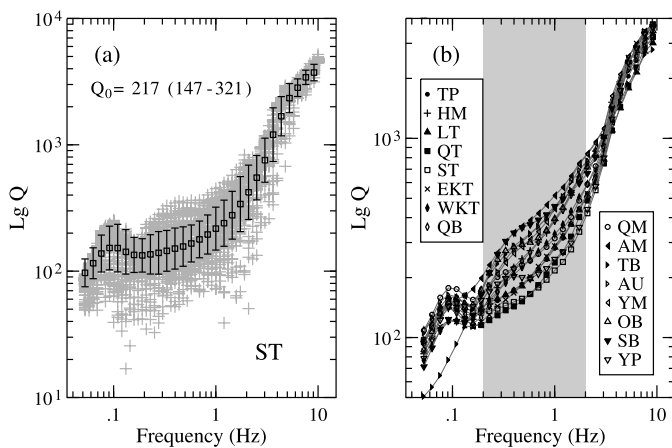
4. The possible crustal flow pattern constrained by Lg attenuation

The partially molten layer in the middle or lower crust is generated by the continental crust thickening and behaves like a fluid over the formation time scale of the Tibetan Plateau (e.g., Nelson et al., 1996). It is expected that the crustal flow is characterized by low viscosity, high temperature and partial melting. Several high-attenuation regions are observed in the crust and upper mantle in the Tibetan Plateau. Theoretical models and laboratory measurements show that strong seismic attenuation is usually an indicator of high temperatures and partial melts. Therefore, we try to use regional Lg-wave attenuation distributions to constrain the possible Tibetan Plateau crustal flow pattern. Illustrated in Fig. 6a is a

Table 1

Lg Q models for individual geological blocks.

Geological block	Block name	CRUST2.0 Crustal thickness	Q_0 (1 Hz Q)	Broadband Q (0.2–2.0 Hz)	Pn velocity (km/s)	Type of blocks
The Tibetan Plateau (> 4 km)	TP	64.1 ± 7.8	280 (194–406)	220 (153–316)	8.04 ± 0.07	Integrated
Himalaya	HM	63.6 ± 7.1	386 (315–473)	291 (245–345)	8.07 ± 0.05	Mountains
Lhasa terrane	LT	65.9 ± 11.4	284 (214–378)	220 (159–303)	8.03 ± 0.08	Integrated
Qiangtang terrane	QT	67.0 ± 8.1	238 (171–332)	185 (136–251)	8.00 ± 0.05	Integrated
Songpan–Ganzi–Hoh xil terrane	ST	57.8 ± 7.7	217 (147–321)	182 (129–256)	8.00 ± 0.05	Integrated
Eastern Kunlunshan terrane	EKT	59.0 ± 4.4	289 (223–374)	218 (160–298)	8.10 ± 0.06	Mountains
Western Kunlunshan terrane	WKT	60.7 ± 5.1	330 (263–414)	259 (212–316)	8.00 ± 0.06	Mountains
Qaidam basin	QB	57.9 ± 2.5	385 (273–544)	281 (201–395)	8.16 ± 0.03	Basin
Qilianshan mountains	QM	51.4 ± 5.3	315 (252–393)	265 (204–345)	8.11 ± 0.06	Mountains
Altyn Tagh mountains	AM	51.8 ± 2.4	517 (439–607)	397 (342–461)	8.15 ± 0.04	Mountains
Tarim basin	TB	51.1 ± 3.6	443 (388–506)	346 (301–397)	8.13 ± 0.06	Basin
Alashan uplift	AU	49.4 ± 3.2	452 (394–518)	343 (304–386)	8.11 ± 0.06	Mountains
Yinshan mountains	YM	43.0 ± 3.7	444 (385–512)	335 (300–374)	7.91 ± 0.21	Mountains
Ordos basin	OB	41.3 ± 2.4	395 (328–476)	328 (283–381)		Basin
Sichuan basin	SB	40.6 ± 2.3	456 (425–489)	370 (343–398)	8.06 ± 0.05	Basin
Yungui plateau	YP	43.0 ± 1.2	247 (184–333)	221 (159–305)	8.02 ± 0.04	Integrated

**Fig. 4.** (a) Frequency-dependent Q_{Lg} for the Songpan–Ganzi–Hoh xil terrane (ST), and (b) the Q_{Lg} versus frequency for different geo-blocks.

map of Q_{Lg} (0.2–2.0 Hz), along with the main fault systems (light-blue lines) and geo-tectonics (white lines). Red contours in Fig. 6a delimit the heavily attenuated regions with Q_{Lg} (0.2–2.0 Hz) < 200. A low- Q_{Lg} belt is distributed along the northern and eastern borders of the Tibetan Plateau. Based on this pattern, the main flow channel appears starting from the north and moves eastward. Then, the channel turns toward southeastern Tibet, moving along the western edge of the rigid Sichuan basin. After passing the narrow channel, it spreads to a wide front. In addition to the main flow channel, there may be another channel, which starts from southern Tibet, crosses the Eastern Himalayan syntaxis, and merges with the main channel.

Shown in Fig. 6b is the Pn velocity in the Tibetan Plateau and surrounding areas (Liang and Song, 2006). Comparing Figs. 6a and 6b, the Lg-wave attenuation and Pn velocity are generally correlated, with high attenuations being related to low Pn velocities. Normally, the Q_{Lg} reflects the material properties in the crust, while the Pn velocity is related to the properties in the uppermost mantle. Investigating the distributions of both Q_{Lg} and the Pn velocity anomalies can provide information on the depth dependence of subsurface processes. For the main flow channel, both strong Lg-wave attenuation and low Pn-velocity anomalies are observed, suggesting it happened at greater depth. However, for the second flow channel, although there are strong Lg-wave attenuations, no Pn-velocity anomaly is observed, suggesting it occurred at a much shallower depth. These findings are consistent with the previous observations (Beaumont et al., 2004; Clark and Royden, 2000;

Fan and Lay, 2003a; Nelson et al., 1996; Owens and Zandt, 1997; Royden et al., 2008; Xie et al., 2004).

Based on the geophysical evidence, Klemperer (2006) suggested the active flow patterns shown in Fig. 6, where black open arrows indicate the middle- or lower-crust flow directions, while the black open circles mark the regions with no flow. The north–south compression and east–west extension of Tibet drive an eastward flow beneath the Qiangtang and Songpan–Ganzi–Hoh xil terranes. This flow bifurcates north and south of the rigid Sichuan basin. The gravitational potential energy and orographic exhumation drive a southward flow between the subducting Indian lower lithosphere and the brittle upper crusts of the Himalaya and southern Lhasa terrane. Bai et al. (2010) produced magnetotelluric images showing two major zones or channels of high electrical conductivity located at depths 20–40 km and extended horizontally for more than 800 km from the Tibetan Plateau to the Yungui Plateau. Using blue arrows, we superimpose their flow model on both the Q_{Lg} and the Pn velocity maps in Fig. 6. The first high conductivity channel is roughly consistent with the regions having both strong attenuation and low Pn-velocity anomalies. Comparing crustal flow patterns proposed by Bai et al. (2010) based on their magnetotelluric data (blue arrows in Fig. 6) with the flow channels constrained by our Q_{Lg} data, both of them share a similar flow trend although their locations are not exactly correlated. In their magnetotelluric observations crossing the eastward low- Q_{Lg} branch, Bai et al. (2010) did not find any high conductivity layer. However, their magnetotelluric observation did find a flow channel, which stretching from southern to southeastern Tibet, moving clockwise around the eastern Himalayan. This flow channel is consistent with the regional structural trend (e.g., Molnar and Lyoncaen, 1989) and roughly correlates to our second flow channel.

5. Discussion

The Q_{Lg} variation can result from the physical properties and thermal status of the crust, or be affected by the geometrical parameters of the crustal waveguide such as the change of the crust thickness (Zhang and Lay, 1995). Zhao et al. (2010, 2013) investigated the relationship between the low-frequency Q_{Lg} and the crust thickness in Northeast China and North China Craton, and found a tendency that the Q_{Lg} is usually high for regions with thicker crust. However, the Tibetan plateau is characterized by unusually thick crust and very low Q_{Lg} making it unique and should not be fit into a conventional crust model. To compare the Tibetan data with those from other regions, illustrated in Fig. 7 is Q_{Lg} versus the crust thickness. The triangles and squares are data from the Northeast China and North China Craton (Zhao et al., 2010, 2013).

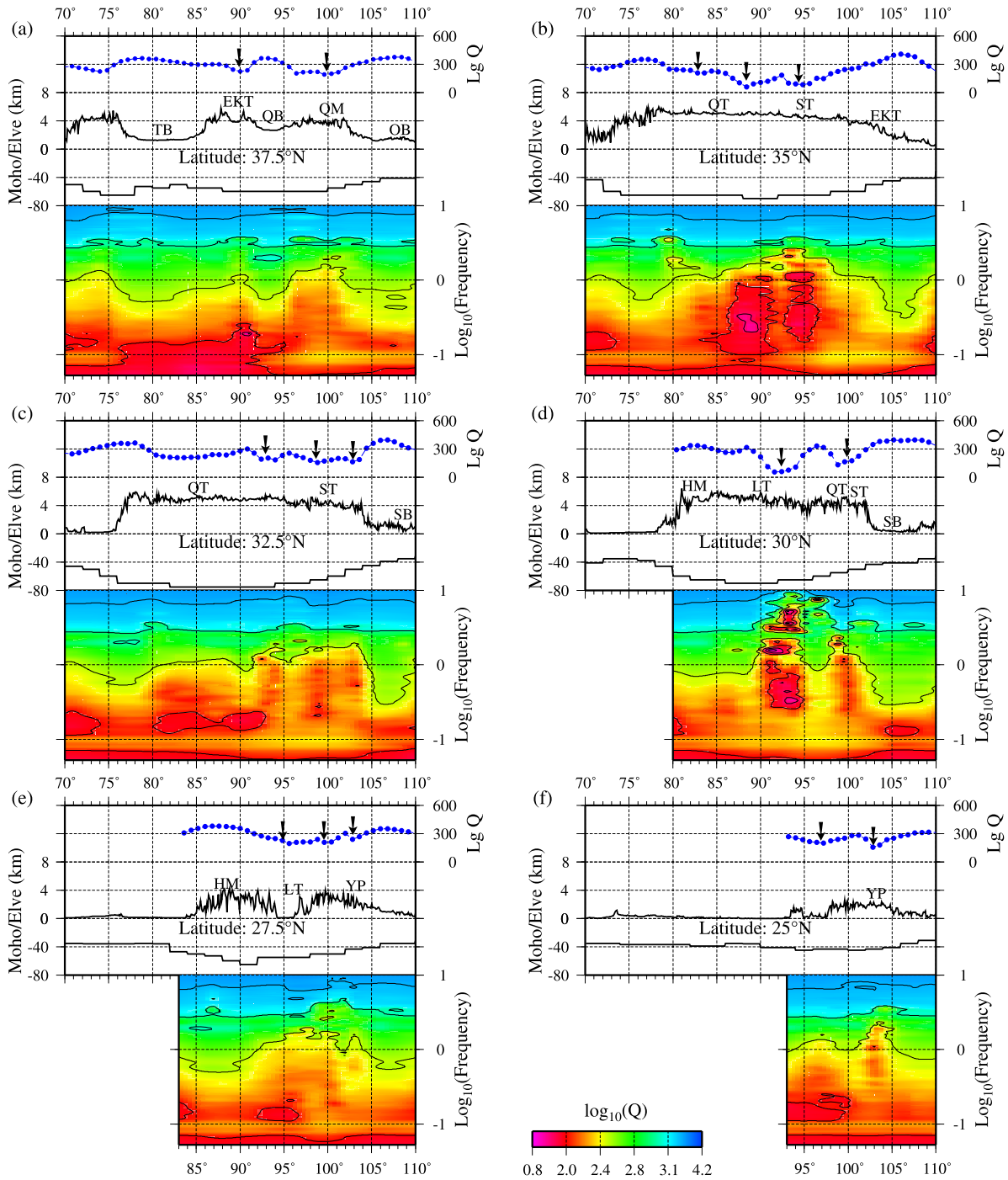


Fig. 5. Selected cross sections of the broadband Q_{Lg} . Upper part, comparison of average Q_{Lg} , surface topography, and Moho depth. Lower part, the Q_{Lg} versus frequency. The horizontal coordinate is longitude and latitude is labeled in the figure. Details refer to the text.

These data are averaged values between 0.2 and 1.0 Hz and from large regions rather than small geology units, thus are relatively stable and representative. To compare with these results, the Q_{Lg} from different parts of Tibetan Plateau and its vicinity are averaged in the same frequency band and shown in the figure as circles. The NEC and NCC data are mostly located at the upper-left in the figure, having relatively thin crust and high Q_{Lg} values, and forming a rough relationship shown by a dashed line with high Q_{Lg} values correlate to thicker crust. On the contrary, the data from the major part of the Tibetan Plateau (circled by the dashed line) are characterized by very thick crust of 57 to 67 km and low average Q_{Lg} from 163 to 254. The group of data circled by the dotted line

comes from stable basins and rigid mountain areas surrounding the Tibetan Plateau (refer to Fig. 1). They have average crust thicknesses between 40 and 52 km and average Q_{Lg} from 292 to 363. The shaded symbols mark the centroids of different data groups, where triangle and square are for the entire NEC and entire NCC, and the two shaded circles are for the part of Tibet with elevations large than 4000 m and the stable regions surrounding the plateau.

Fig. 7 suggests that the dominant mechanisms of the Lg-wave attenuation in the major Tibetan Plateau differ from those in other regions. Possibly, the strong thermal activities and heterogeneities from partially melted magma chambers make both intrinsic and scattering attenuations very effective. At the same time, bumpy

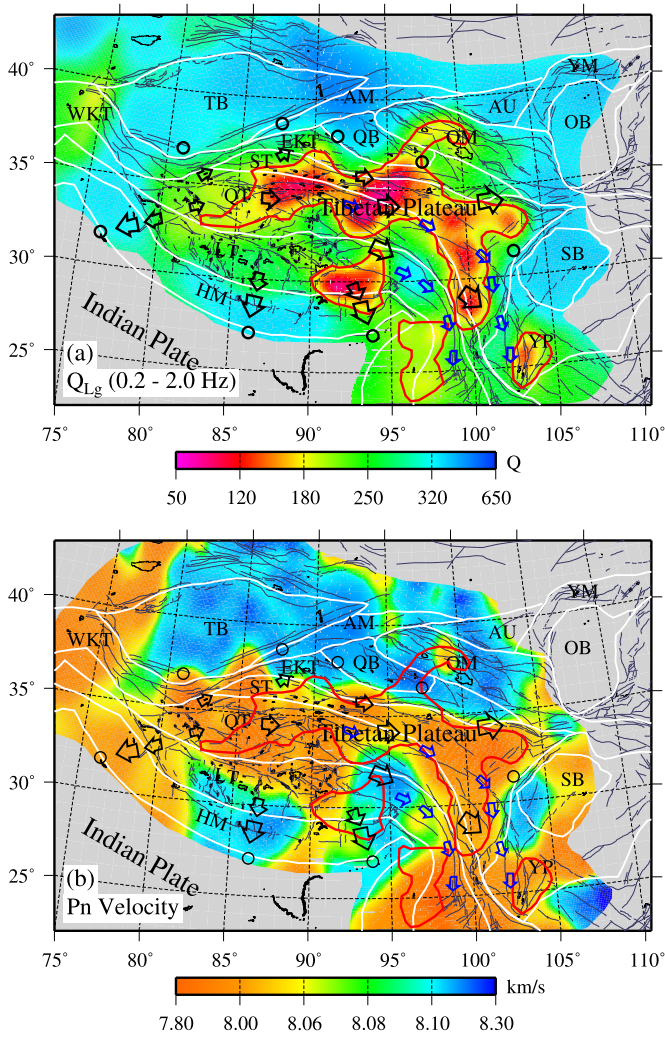


Fig. 6. Comparison between (a) the average Q_{Lg} (over 0.2–2.0 Hz) and (b) the Pn velocity in the Tibetan Plateau and surrounding regions. Also shown in the figure are main fault systems (light-blue lines) and regional tectonics (white lines). Note that the red lines are $Q_{Lg} = 200$ contours which delimit the high attenuation areas. Details refer to the text.

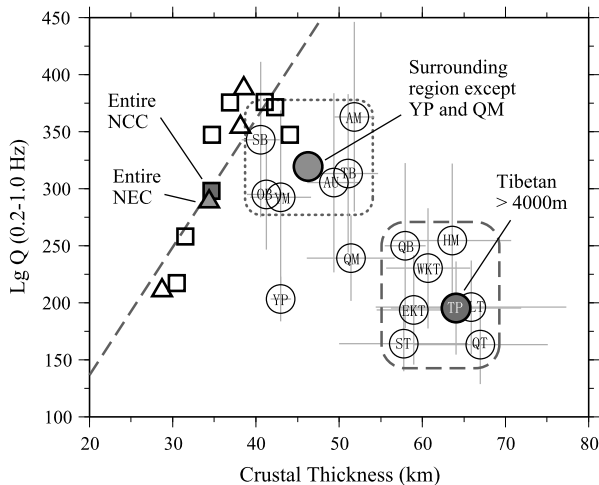


Fig. 7. The average Q_{Lg} versus the average crustal thickness for selected geology units in the Tibetan Plateau and its vicinity. The data from the major part of the Tibetan Plateau are circled by the dashed line. The data from regions surrounding the Tibetan Plateau are circled by the dotted line. As comparisons, the Q_{Lg} values from other regions in China (triangles and squares) are also included in the figure. Details refer to the text.

topography, weaker Moho discontinuity and possibly the double-layered thick crust are all unfavorable for the propagation of Lg as a guided wave. The data from stable regions surrounding the plateau have thicker crust and slightly lower Q_{Lg} compared to the NEC and NCC data. However, their crust thickness and Q_{Lg} are still different from those in the major Tibetan Plateau. There are two exceptional blocks, the YP and QM, which cannot be assigned to either group. Compared to other regions surrounding the major Tibetan Plateau, the YP and QM have similar crust thickness but their Q_{Lg} are about 100 lower. What causes this is still not fully understood but the YP and QM are two weakest areas surrounding the major Tibetan Plateau. Due to the combined effect of the subducting India Plate and strong holding of the Eurasia Plate at TB, QB, OB and SB, the crust and upper mantle material in Tibetan Plateau could be streamed out in between these rigid basins. It has been suggested by previous authors that the YP and QM are two possible paths of material out flow (e.g., Wang et al., 2013; Zhang et al., 2011). It is possible that the crusts in these narrow paths underwent strong shear movement and are highly heterogeneous, which causes additional attenuation.

Fig. 8 summarizes the geology and attenuation in a north–south profile along longitude 93° E. Shown in Figs. 8a and 8b are cartoons depicting the surface topography with geological sutures as well as the crust and upper mantle structures adapted from Jin et al. (1996), Owens and Zandt (1997), Kosarev et al. (1999), Kind et al. (2002), and DeCelles et al. (2002). The broadband Q_{Lg} versus frequency are shown in Fig. 8c (note the vertical coordinate is the frequency). Overlapped on the generally smoothed background attenuation, there are three absorbing bands labeled with ①–③. If scattering dominates the Lg-wave attenuation, the maximum absorbing happens at $ka = 1$, where k is the wavenumber and a is the dominant scale of the scatters either in the crustal waveguide (Wu et al., 2000) or at the surface (He et al., 2008). Thus, the absorbing band may provide information regarding the scales of heterogeneities. In Fig. 8c, the high-frequency absorbing band ① is located near the northern Himalaya and southern Lhasa terrane. Its frequency band of 2.0 to 10.0 Hz corresponds to small scatters of 60 m to 300 m. Numerous geothermal systems were found in this region (Hochstein and Regenauer-Lieb, 1998). Heat-flow measurements show large variations over a short distance in southernmost Tibet. For example, Francheteau et al. (1984) reported that the heat flow decreases sharply from 146 to 91 mW/m² over a distance less than 25 km between the southern and northern lakes near the Kangmar domain. The sharp heat flow variations suggest that the regional melting conditions are met at relatively shallow depths in the Tibetan crust. Xie et al. (2004) found a strong crustal Lg-wave attenuation in the Yangbajing graben, and suggested that the attenuation resulted from hydrothermal and magmatic fluids in the upper crust. The absorbing band ② is located in southern Tibet between 28° and 31° N. This area coincides with a series of bright spots found from reflection surveys (Brown et al., 1996; Makovsky et al., 1996; Nelson et al., 1996). These bright spots are located at depths of approximately 15 km and are interpreted to be the top of a low P-velocity layer. Makovsky and Klemperer (1999) used AVO (amplitude versus offset) modeling to constrain the P and S velocities of these spots to be 3.0 ± 0.8 and 1.6 ± 0.8 km/s, respectively, and suggested that the spots were caused by aqueous fluid concentrations that are underlain by partially molten layers. These layers are also characterized by low S velocities (Cotte et al., 1999; Guo et al., 2009; Kind et al., 2002; Rapine et al., 2003), high electromagnetic conductivities (Li et al., 2003; Unsworth et al., 2005), high conductive heat flow (Francheteau et al., 1984; Hochstein and Regenauer-Lieb, 1998) and strong crustal attenuation (Fan and Lay, 2003a; Xie et al., 2004), all suggesting that a minimum-strength layer could exist in the mid-to-lower crust where modern day rhe-

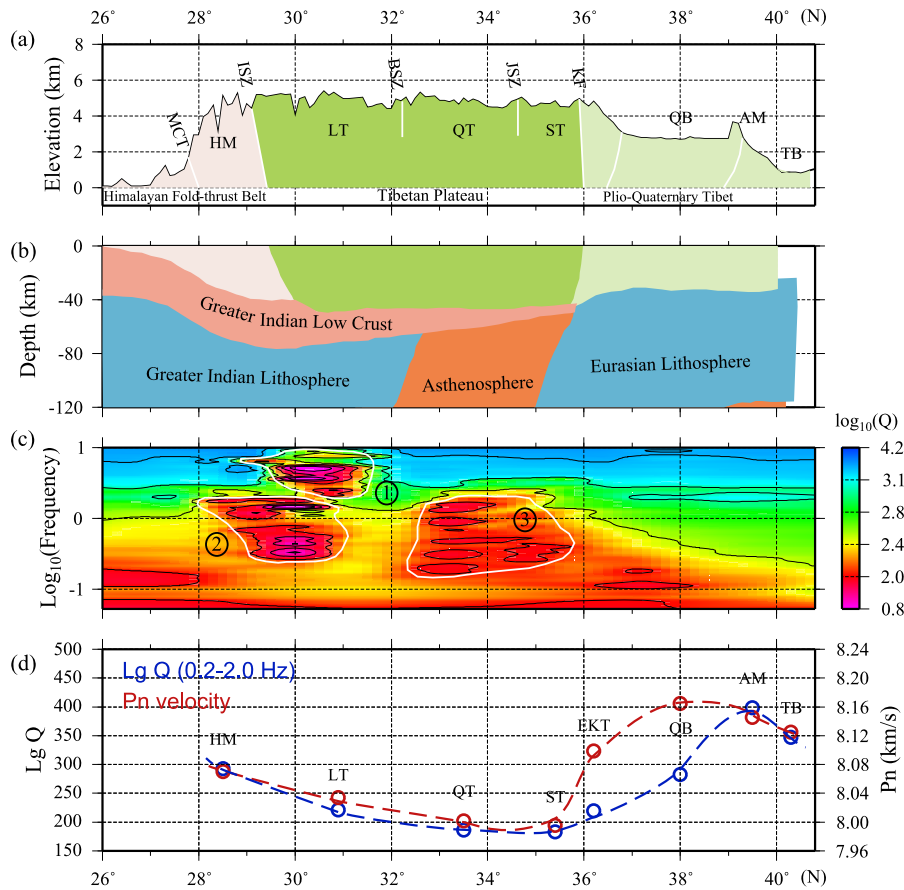


Fig. 8. A combined longitudinal cross section along 93° E, with (a) surface topography, (b) schematic crust and upper mantle structure, (c) $\log(Q_{lg})$ versus frequency, and (d) comparison between average $Lg Q$ and average Pn velocity for selected geology units. Details refer to the text.

ological flow is likely occurring (Klemperer, 2006). The dominate frequency of the strong attenuation is between 0.25 to 2.0 Hz, suggesting heterogeneities of 0.3 km to 2.5 km. The absorbing band ③ spans a distance of approximately 400 km under the Qiangtang and Songpan–Ganzi–Hoh xil terranes. The dominant frequency of this absorbing band is 0.15 to 2.0 Hz, which corresponds to heterogeneity scales between 0.3 km and 4 km. This is the most volcanically active area in Tibet (e.g., Molnar, 1989; Turner et al., 1993). Owens and Zandt (1997) found a lower crustal low-velocity zone with a high Poisson's ratio of ~ 0.35 in this region and suggested that it likely involves partial melt.

The major geology units in the Tibetan Plateau are aligned in east–west direction and gradually turn to southeast at the east end of the plateau. In Fig. 8d, we roughly project their $Q_{lg}(0.2\text{--}2.0\text{ Hz})$ values and Pn velocities to the 93° E profile. These average values come from vast areas thus should reflect the behavior of these structures sequentially placed in front of the collision of the Indian Plate. From south to north, the average Q_{lg} changes by first decrease and then increase. At the southern end, the average Q_{lg} for the Himalaya Mountains (HM) are around 300. The lowest average Q_{lg} of 182–185 appear in the Qiangtang (QT) and Songpan–Ganzi–Hoh xil terranes (ST). It reaches to 281 in the Qaidam basin (QB) and reaches to 397 and 346 in AM and TB. The Pn velocity variation resembles that of the attenuation with its lowest value occurs at QT and ST. Towards north, at EKT and QB, the Pn velocity raises abruptly before the increase of the Q_{lg} by approximately 2° or 200 km. At the northern edge, both Q_{lg} and Pn velocity finally reach to their normal values at AM and TB. This can also be seen in Fig. 6, where the warm colored low Q region extends further north than the warm colored low Pn velocity. If the Pn velocity reflects deeper activities compared to crustal attenuation, Fig. 8d

may give the hint that the shallow activities extended to further north than deeper activities.

6. Conclusion

We obtained a 0.05–10.0 Hz broadband high-resolution Lg -wave attenuation model in the Tibetan Plateau and its surrounding regions. The best data coverage was in the Tibetan Plateau and between 0.05 and 1.5 Hz, where the Q_{lg} model has a resolution of approximately $1^\circ \times 1^\circ$. Regions with strong attenuations were found in the Tibetan Plateau. These results were consistent with previous works but have higher resolution and broader frequency band, making it possible to investigate many relations between the attenuation and detailed regional tectonics. The directly inverted Lg -wave attenuations were relatively scattered. To obtain reliable results, we calculated mean values of Q_{lg} at different tectonic units. The resulted statistical relations were much more stable and robust to characterize the regional geology. By analyzing the regional variations of low-frequency Q_{lg} versus the crustal thickness in Tibetan Plateau, and comparing them with those found in North China Craton and Northeast China, we found that the major Tibetan plateau is characterized by unusually thick crust and low Q_{lg} , suggesting the dominant attenuation mechanisms in this area differ from those in other regions. Strong seismic attenuation is usually an indicator of underlying processes involving high temperature and partial melts. Thus, high resolution Q_{lg} distributions provide constrains to the extent of these processes. Based on attenuation measurement, we predicted possible channels of crustal material flow beneath the Tibetan Plateau. The main flow channel appeared starting from the northern end of plateau, stretching

toward east and southeast, and then turned to south after been blocked by the rigid Sichuan Basin.

Acknowledgements

We thank Prof. T. Lay for many discussions and comments on this work. Two anonymous reviewers are appreciated for their constructive comments that greatly improved this manuscript. The broadband data used in this study were retrieved from the China Earthquake Networks Center (CENC), the Data Management Centre of China National Seismic Network at the Institute of Geophysics, the China Earthquake Administration (Zheng et al., 2010), the IRIS Data Management Center, and the NEIC. The Pn-velocities used in Fig. 6b were provided by Dr. C. Liang. Some figures were created using the GMT (Wessel and Smith, 1998). This research was supported by the National Natural Science Foundation of China (grants 40974029, 41174048 and 41074041). X.B.X. wishes to thank AFRL for support under grant FA9453-11-C-0234.

Appendix A. Supplementary material

Supplementary material related to this article can be found online at <http://dx.doi.org/10.1016/j.epsl.2013.09.038>.

References

- Bai, D.H., Unsworth, M.J., Meju, M.A., Ma, X.B., Teng, J.W., Kong, X.R., Sun, Y., Sun, J., Wang, L.F., Jiang, C.S., Zhao, C.P., Xiao, P.F., Liu, M., 2010. Crustal deformation of the eastern Tibetan plateau revealed by magnetotelluric imaging. *Nat. Geosci.* 3, 358–362, <http://dx.doi.org/10.1038/NGEO830>.
- Bao, X.Y., Sandvol, E., Ni, J., Hearn, T., Chen, Y.S.J., Shen, Y., 2011. High resolution regional seismic attenuation tomography in eastern Tibetan Plateau and adjacent regions. *Geophys. Res. Lett.* 38, L16304, <http://dx.doi.org/10.1029/2011GL048012>.
- Bassin, C., Laske, G., Masters, G., 2000. The current limits of resolution for surface wave tomography in North America. *Eos Trans. AGU* 81, F897.
- Beaumont, C., Jamieson, R.A., Nguyen, M.H., Medvedev, S., 2004. Crustal channel flows: 1. Numerical models with applications to the tectonics of the Himalayan–Tibetan orogen. *J. Geophys. Res.* 109, B06406, <http://dx.doi.org/10.1029/2003JB002809>.
- Brown, L.D., Zhao, W.J., Nelson, D.K., Hauck, M., Alsdorf, D., Ross, A., Cogan, M., Clark, M., Liu, X.W., Che, J.K., 1996. Bright spots, structure, and magmatism in southern Tibet from INDEPTH seismic reflection profiling. *Science* 274, 1688–1690.
- Clark, M.K., Royden, L.H., 2000. Topographic ooze: Building the eastern margin of Tibet by lower crustal flow. *Geology* 28, 703–706.
- Cotte, N., Pedersen, H., Campillo, M., Mars, J., Ni, J.F., Kind, R., Sandvol, E., Zhao, W., 1999. Determination of the crustal structure in southern Tibet by dispersion and amplitude analysis of Rayleigh waves. *Geophys. J. Int.* 138, 809–819.
- DeCelles, P.G., Robinson, D.M., Zandt, G., 2002. Implications of shortening in the Himalayan fold-thrust belt for uplift of the Tibetan Plateau. *Tectonics* 21, 1062, <http://dx.doi.org/10.1029/2001TC001322>.
- Fan, G.W., Lay, T., 2002. Characteristics of Lg attenuation in the Tibetan plateau. *J. Geophys. Res.* 107, <http://dx.doi.org/10.1029/2001JB000804>.
- Fan, G.W., Lay, T., 2003a. Strong Lg attenuation in the Tibetan Plateau. *Bull. Seismol. Soc. Am.* 93, 2264–2272.
- Fan, G.W., Lay, T., 2003b. Strong Lg wave attenuation in the Northern and Eastern Tibetan Plateau measured by a two-station/two-event stacking method. *Geophys. Res. Lett.* 30, <http://dx.doi.org/10.1029/2002GL016211>.
- Flesch, L.M., Haines, A.J., Holt, W.E., 2001. Dynamics of the India–Eurasia collision zone. *J. Geophys. Res.* 106, 16435–16460.
- Francheteau, J., Jaupart, C., Shen, X.J., Kang, W.H., Lee, D.L., Bai, J.C., Wei, H.P., Deng, H.Y., 1984. High heat-flow in southern Tibet. *Nature* 307, 32–36.
- Guo, Z., Gao, X., Yao, H.J., Li, J., Wang, W.M., 2009. Midcrustal low-velocity layer beneath the central Himalaya and southern Tibet revealed by ambient noise array tomography. *Geochim. Geophys. Res.* 10, <http://dx.doi.org/10.1029/2009gc002458>.
- He, Y.F., Xie, X.B., Lay, T., 2008. Explosion-source energy partitioning and Lg-wave excitation: Contributions of free-surface scattering. *Bull. Seismol. Soc. Am.* 98, 778–792.
- Heidbach, O., Tingay, M., Barth, A., Reinecker, J., Kurfess, D., Müller, B., 2010. Global crustal stress pattern based on the world stress map database release 2008. *Tectonophysics* 482, 3–15, <http://dx.doi.org/10.1016/j.tecto.2009.07.023>.
- Hochstein, M.P., Regenauer-Lieb, K., 1998. Heat generation associated with collision of two plates: the Himalayan geothermal belt. *J. Volcanol. Geotherm. Res.* 83, 75–92.
- Jin, Y., McNutt, M.K., Zhu, Y.S., 1996. Mapping the descent of Indian and Eurasian plates beneath the Tibetan Plateau from gravity anomalies. *J. Geophys. Res.* 101, 11275–11290.
- Kind, R., Yuan, X., Saul, J., Nelson, D., Sobolev, S.V., Mechie, J., Zhao, W., Kosarev, G., Ni, J., Achauer, U., Jiang, M., 2002. Seismic images of crust and upper mantle beneath Tibet: Evidence for Eurasian plate subduction. *Science* 298, 1219–1221.
- Klemperer, L.S., 2006. Crustal flow in Tibet: geophysical evidence for the physical state of Tibetan lithosphere, and inferred patterns of active flow. In: Law, R.D., Searle, M.P., Godin, L. (Eds.), *Geol. Soc. Spec. Publ. Geological Society, London*, pp. 39–70. Special publications.
- Kosarev, G., Kind, R., Sobolev, S.V., Yuan, X., Hanka, W., Oreshin, S., 1999. Seismic evidence for a detached Indian lithospheric mantle beneath Tibet. *Science* 283, 1306–1309.
- Langille, J., Lee, J., Hacker, B., Seward, G., 2010. Middle crustal ductile deformation patterns in southern Tibet: Insights from vorticity studies in Mabja Dome. *J. Struct. Geol.* 32, 70–85.
- Li, S.H., Unsworth, M.J., Booker, J.R., Wei, W.B., Tan, H.D., Jones, A.G., 2003. Partial melt or aqueous fluid in the mid-crust of Southern Tibet? Constraints from INDEPTH magnetotelluric data. *Geophys. J. Int.* 153, 289–304.
- Li, C., Van der Hilst, R.D., Meltzer, A.S., Engdahl, E.R., 2008. Subduction of the Indian lithosphere beneath the Tibetan Plateau and Burma. *Earth Planet. Sci. Lett.* 274, 157–168.
- Liang, C.T., Song, X.D., 2006. A low velocity belt beneath northern and eastern Tibetan Plateau from Pn tomography. *Geophys. Res. Lett.* 33, L22306, <http://dx.doi.org/10.1029/2006GL027926>.
- Liu, M.J., Mooney, W.D., Li, S.L., Okaya, N., Detweiler, S., 2006. Crustal structure of the northeastern margin of the Tibetan plateau from the Songpan–Ganzi terrane to the Ordos basin. *Tectonophysics* 420, 253–266, <http://dx.doi.org/10.1016/j.tecto.2006.01.025>.
- Makovsky, Y., Klemperer, S.L., 1999. Measuring the seismic properties of Tibetan bright spots: Evidence for free aqueous fluids in the Tibetan middle crust. *J. Geophys. Res.* 104, 10795–10825.
- Makovsky, Y., Klemperer, S.L., Ratschbacher, L., Brown, L.D., Li, M., Zhao, W.J., Meng, F.L., 1996. INDEPTH wide-angle reflection observation of P-wave-to-S-wave conversion from crustal bright spots in Tibet. *Science* 274, 1690–1691.
- McNamara, D.E., Owens, T.J., Silver, P.G., Wu, F.T., 1994. Shear-wave anisotropy beneath the Tibetan Plateau. *J. Geophys. Res.* 99, 13655–13665.
- Molnar, P., 1989. The geologic evolution of the Tibetan Plateau. *Am. Sci.* 77, 350–360.
- Molnar, P., Lyoncaen, H., 1989. Fault plane solutions of earthquakes and active tectonics of the Tibetan Plateau and its margins. *Geophys. J. Int.* 99, 123–153.
- Nelson, K.D., Zhao, W.J., Brown, L.D., Kuo, J., Che, J.K., Liu, X.W., Klemperer, S.L., Makovsky, Y., Meissner, R., Mechie, J., Kind, R., Wenzel, F., Ni, J., Nabelek, J., Chen, L.S., Tan, H.D., Wei, W.B., Jones, A.G., Booker, J., Unsworth, M., Kidd, W.S.F., Hauck, M., Alsdorf, D., Ross, A., Cogan, M., Wu, C.D., Sandvol, E., Edwards, M., 1996. Partially molten middle crust beneath southern Tibet: Synthesis of project INDEPTH results. *Science* 274, 1684–1688.
- Ni, J., Barazangi, M., 1983. High-frequency seismic-wave propagation beneath the Indian shield, Himalayan arc, Tibetan plateau and surrounding regions: High uppermost mantle velocities and efficient Sn propagation beneath Tibet. *Geophys. J. R. Astron. Soc.* 72, 665–689.
- Owens, T.J., Zandt, G., 1997. Implications of crustal property variations for models of Tibetan plateau evolution. *Nature* 387, 37–43.
- Rai, S.S., Ashish, Padhi, A., Sarma, P.R., 2009. High crustal seismic attenuation in Ladakh–Karakoram. *Bull. Seismol. Soc. Am.* 99, 407–415.
- Rapine, R., Tilmann, F., West, M., Ni, J., Rodgers, A., 2003. Crustal structure of northern and southern Tibet from surface wave dispersion analysis. *J. Geophys. Res.* 108, 2120, <http://dx.doi.org/10.1029/2001jb000445>.
- Rodgers, A.J., Schwartz, S.Y., 1998. Lithospheric structure of the Qiangtang Terrane, northern Tibetan Plateau, from complete regional waveform modeling: Evidence for partial melt. *J. Geophys. Res.* 103, 7137–7152.
- Royden, L.H., Burchfiel, B.C., van der Hilst, R.D., 2008. The geological evolution of the Tibetan Plateau. *Science* 321, 1054–1058, <http://dx.doi.org/10.1126/science.1155371>.
- Searle, M.P., Elliott, J.R., Phillips, R.J., Chung, S.L., 2011. Crustal–lithospheric structure and continental extrusion of Tibet. *J. Geol. Soc. (Lond.)* 168, 633–672, <http://dx.doi.org/10.1144/0016-76492010-139>.
- Shapiro, N.M., Ritzwoller, M.H., Molnar, P., Levin, V., 2004. Thinning and flow of Tibetan crust constrained by seismic anisotropy. *Science* 305, 233–236.
- Turner, S., Hawkesworth, C., Liu, J.Q., Rogers, N., Kelley, S., Vancalsteren, P., 1993. Timing of Tibetan uplift constrained by analysis of volcanic rocks. *Nature* 364, 50–54.
- Unsworth, M.J., Jones, A.G., Wei, W., Marquis, G., Gokarn, S.G., Spratt, J.E., INDEPTH-MT team, 2005. Crustal rheology of the Himalaya and southern Tibet inferred from magnetotelluric data. *Nature* 438, 78–81, <http://dx.doi.org/10.1038/nature04154>.
- Wang, Q., Gao, Y., Shi, Y., Wu, J., 2013. Seismic anisotropy in the uppermost mantle beneath the northeastern margin of Qinghai–Tibet plateau: evidence from shear wave splitting of SKS, PKS and SKKS. *Chin. J. Geophys.* 56, 892–905, <http://dx.doi.org/10.6038/cjg20130318>.

- Wang, C.Y., Han, W.B., Wu, J.P., Lou, H., Chan, W.W., 2007. Crustal structure beneath the eastern margin of the Tibetan Plateau and its tectonic implications. *J. Geophys. Res.* 112, B07307, <http://dx.doi.org/10.1029/2005JB003873>.
- Wei, W.B., Unsworth, M., Jones, A., Booker, J., Tan, H.D., Nelson, D., Chen, L.S., Li, S.H., Solon, K., Bedrosian, P., Jin, S., Deng, M., Ledo, J., Ray, D., Roberts, B., 2001. Detection of widespread fluids in the Tibetan crust by magnetotelluric studies. *Science* 292, 716–718.
- Wessel, P., Smith, W., 1998. New, improved version of the generic mapping tools released. *Eos* 79, 579.
- Wu, R.S., Jin, S., Xie, X.B., 2000. Energy partition and attenuation of Lg waves by numerical simulations using screen propagators. *Phys. Earth Planet. Inter.* 120, 227–243.
- Xie, J., 2002. Lg Q in the eastern Tibetan Plateau. *Bull. Seismol. Soc. Am.* 92, 871–876.
- Xie, J., Gok, R., Ni, J., Aoki, Y., 2004. Lateral variations of crustal seismic attenuation along the INDEPTH profiles in Tibet from Lg Q inversion. *J. Geophys. Res.* 109, B10308, <http://dx.doi.org/10.1029/2004JB002988>.
- Xu, L.L., Rondenay, S., van der Hilst, R.D., 2007. Structure of the crust beneath the southeastern Tibetan Plateau from teleseismic receiver functions. *Phys. Earth Planet. Inter.* 165, 176–193, <http://dx.doi.org/10.1016/j.pepi.2007.09.002>.
- Yao, H.J., Beghein, C., van der Hilst, R.D., 2008. Surface wave array tomography in SE Tibet from ambient seismic noise and two-station analysis – II. Crustal and upper-mantle structure. *Geophys. J. Int.* 173, 205–219, <http://dx.doi.org/10.1111/j.1365-246X.2007.03696.x>.
- Zhang, Z.J., Deng, Y.F., Teng, J.W., Wang, C.Y., Gao, R., Chen, Y., Fan, W.M., 2011. An overview of the crustal structure of the Tibetan plateau after 35 years of deep seismic soundings. *J. Asian Earth Sci.* 40, 977–989, <http://dx.doi.org/10.1016/j.jseas.2010.03.010>.
- Zhang, T.R., Lay, T., 1995. Why the Lg phase does not traverse oceanic crust. *Bull. Seismol. Soc. Am.* 85, 1665–1678.
- Zhang, P., Shen, Z., Wang, M., Gan, W.J., Burgmann, R., Molnar, P., 2004. Continuous deformation of the Tibetan Plateau from global positioning system data. *Geology* 32, 809–812, <http://dx.doi.org/10.1130/G20554.1>.
- Zhang, Z.J., Yuan, X.H., Chen, Y., Tian, X.B., Kind, R., Li, X.Q., Teng, J.W., 2010. Seismic signature of the collision between the east Tibetan escape flow and the Sichuan Basin. *Earth Planet. Sci. Lett.* 292, 254–264, <http://dx.doi.org/10.1016/j.epsl.2010.01.046>.
- Zhao, L.F., Xie, X.B., Wang, W.M., Zhang, J.H., Yao, Z.X., 2010. Seismic Lg-wave Q tomography in and around Northeast China. *J. Geophys. Res.* 115, B08307, <http://dx.doi.org/10.1029/2009JB007157>.
- Zhao, L.F., Xie, X.B., Wang, W.M., Zhang, J.H., Yao, Z.X., 2013. Crustal Lg-wave attenuation within the North China craton and its surrounding regions. *Geophys. J. Int.* 195 (1), 513–531, <http://dx.doi.org/10.1093/gji/ggt235>.
- Zheng, X.F., Yao, Z.X., Liang, J.H., Zheng, J., 2010. The role played and opportunities provided by IGP DMC of China National Seismic Network in Wenchuan earthquake disaster relief and researches. *Bull. Seismol. Soc. Am.* 100, 2866–2872, <http://dx.doi.org/10.1785/0120090257>.
- Zhou, L.Q., Zhao, C.P., Chen, Z.L., Zheng, S.H., 2011. Amplitude tomography of Lg waves in Xinjiang and its adjacent regions. *Bull. Seismol. Soc. Am.* 101, 1302–1314, <http://dx.doi.org/10.1785/0120100267>.